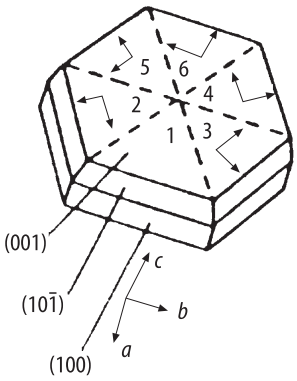

Fig. 41A-4-001. $CsLiSO_4$. The room temperature crystal growth habit composed of six twin domains [88Asa]. The orientations of the crystal *a* and *b* axes for domain 1 are indicated below the figure, while those for domain 2...6 are indicated by small arrows in the domains themselves.

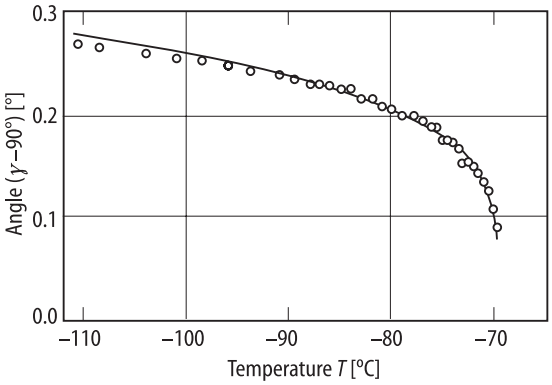

Fig. 41A-4-002. $CsLiSO_4$. ($\gamma - 90°$) vs. T [88Asa]. The solid line represents the relation $(\gamma - 90°) \propto (-69.5 - T)^{0.22}$.

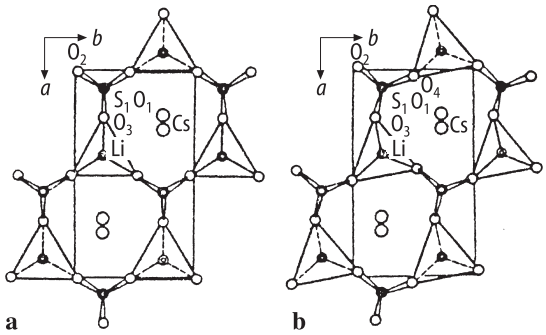

Fig. 41A-4-003. $CsLiSO_4$. Crystal structure of phase I and phase II [79Kru]. Projection along [001]. (**a**) phase I (T = 293 K); (**b**) phase II (T = 163 K). One layer of tetrahedra is shown. A second layer is linked to the first by n-glide symmetry operation.

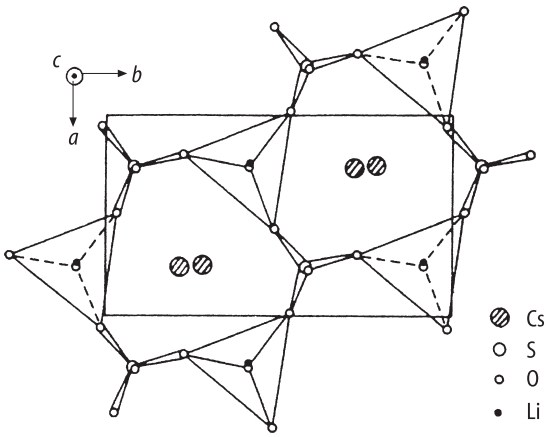

Fig. 41A-4-004. $CsLiSO_4$. Crystal structure of phase II [88Asa]. T = –78 °C. Projection along [001]. One layer of tetrahedra ($z \approx 1/4$) is shown. Configurations with small occupation probability are not drawn.

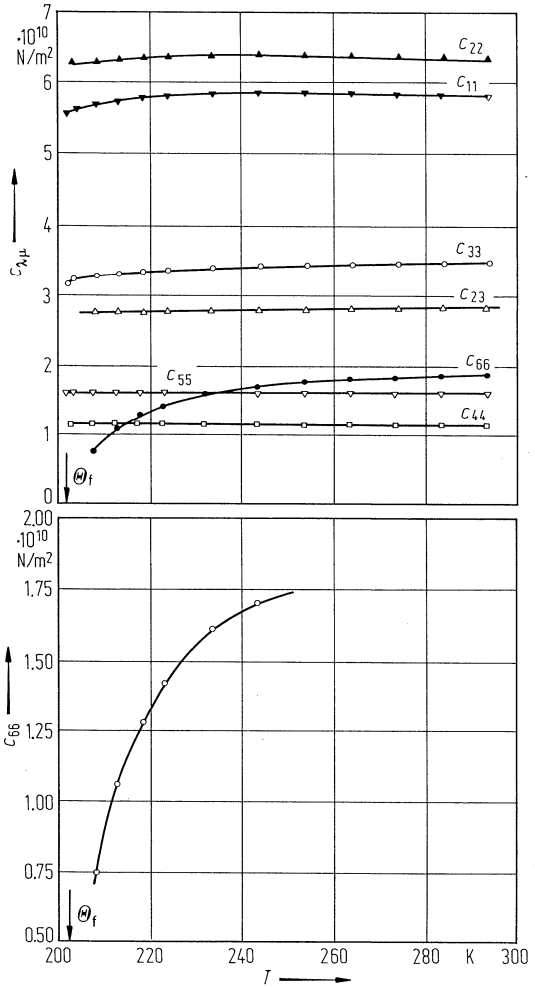

Fig. 41A-4-005. $CsLiSO_4$. $c_{\lambda\mu}$ vs. T [81Ale]. f = 10.0 MHz.

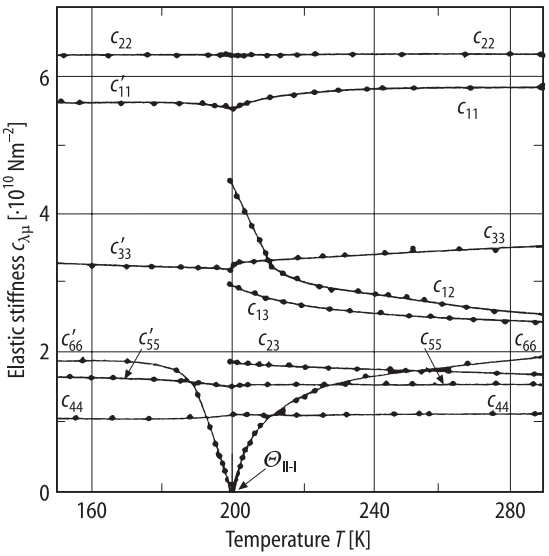

Fig. 41A-4-006. $CsLiSO_4$. $c_{\lambda\mu}$ vs. T [88Mro]. $c_{\lambda\mu}$: elastic stiffness constants obtained by Brillouin scattering.

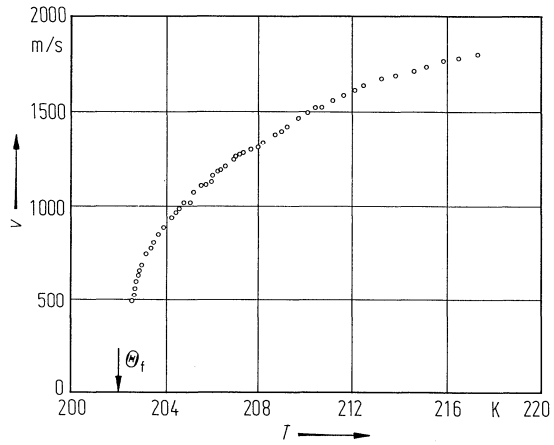

Fig. 41A-4-007. $CsLiSO_4$. υ vs. T [82Oze]. υ: velocity of transverse sound wave. Propagation along [100] with polarization along [010]. f = 3.3 MHz.

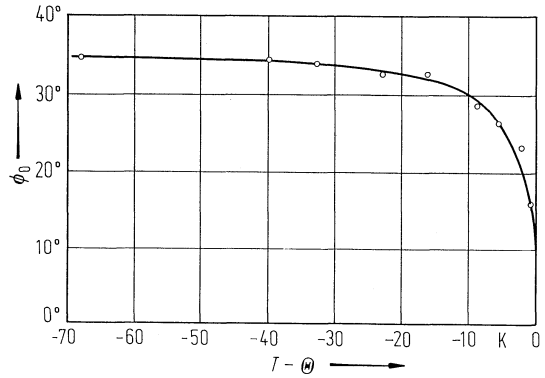

Fig. 41A-4-008. $CsLiSO_4$. ϕ_0 vs. T–Θ [81Pie]. ϕ_0: rotation angle of optical indicatrix. Θ_{II-I} = 203 K.

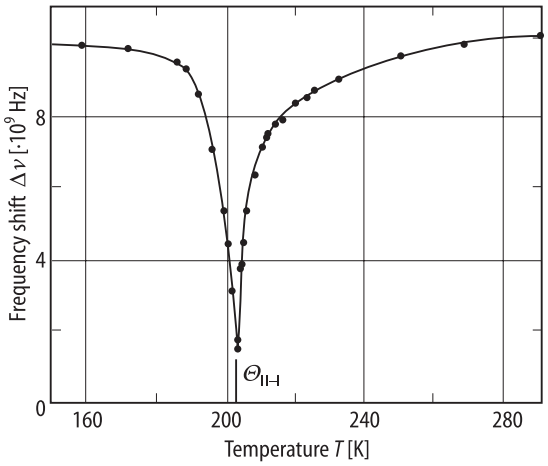

Fig. 41A-4-009. $CsLiSO_4$. $\Delta\nu$ vs. T [88Mro]. $\Delta\nu$: Brillouin scattering of soft acoustic c_{66} mode.

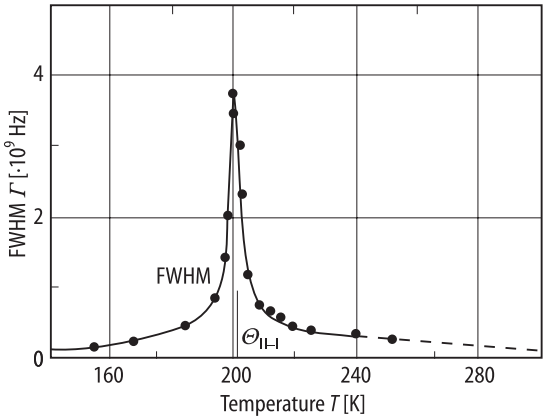

Fig. 41A-4-010. $CsLiSO_4$. Γ vs. T [88Mro]. Γ: full width at half maximum of Brillouin scattering spectrum of soft acoustic c_{66} mode.

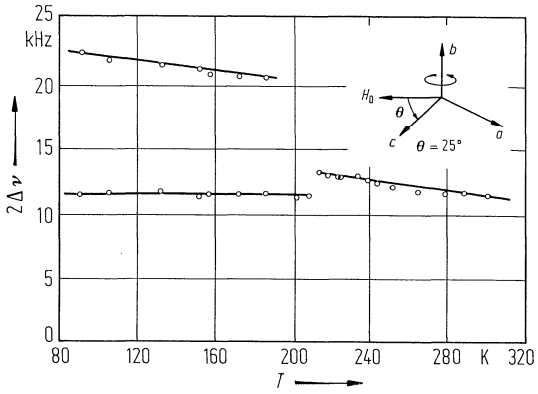

Fig. 41A-4-011. $CsLiSO_4$. $2\Delta\nu$ vs. T [82Roz]. $2\Delta\nu$: quadrupole splitting of ^7Li nuclei.

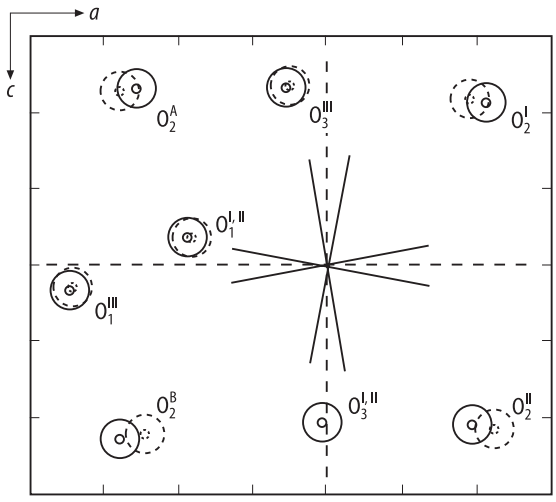

Fig. 41A-4-012. $CsLiSO_4$. Two possible orientations of the electric field gradient tensor of ^{133}Cs on the *ac* plane [86Hol].

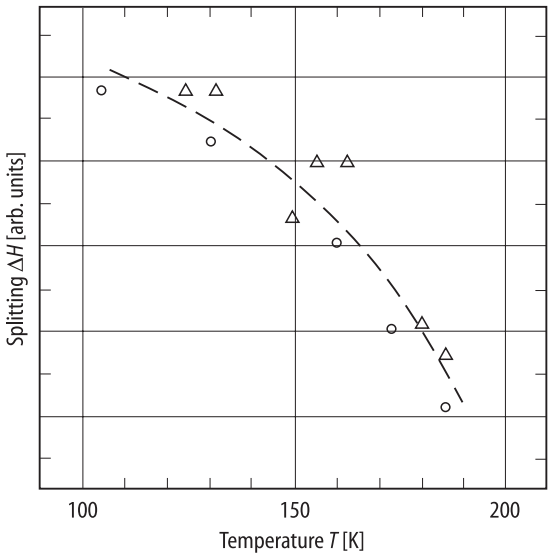

Fig. 41A-4-013. $CsLiSO_4$. ΔH vs. T [86Hol]. ΔH: splitting of the ±5/2 – ±3/2 component of ^{133}Cs at two orientations in the *ab* plane. Open circle and triangle: signals correspond to the two kind of orientations, see Fig. 41A-4-012.

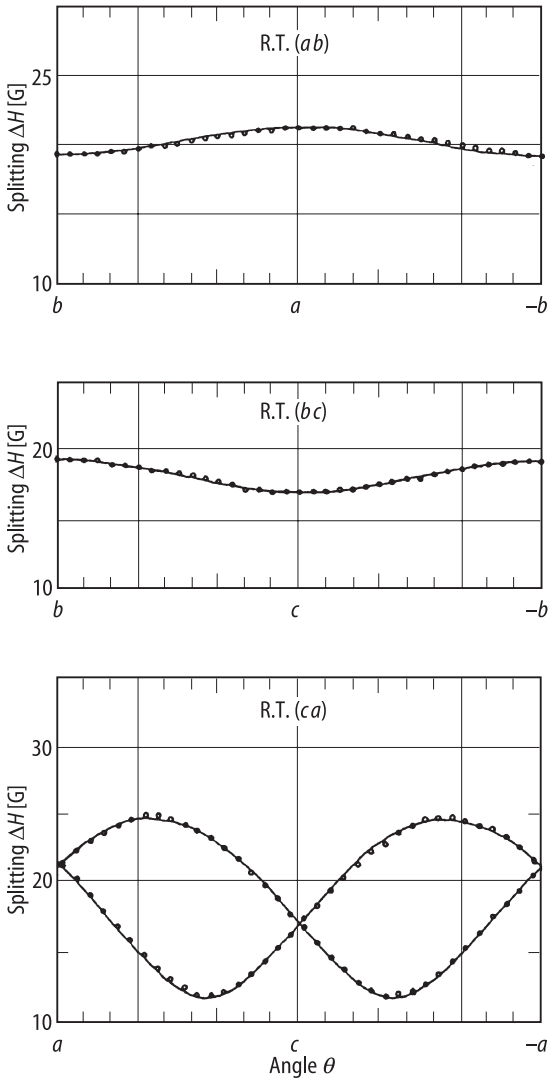

Fig. 41A-4-014. $CsLiSO_4$. ΔH vs. θ [87Hua]. T = RT. ΔH: hyperfine splitting of nitrogen. θ: angle between the magnetic field and crystallographic axes. Solid lines are numerical plot.

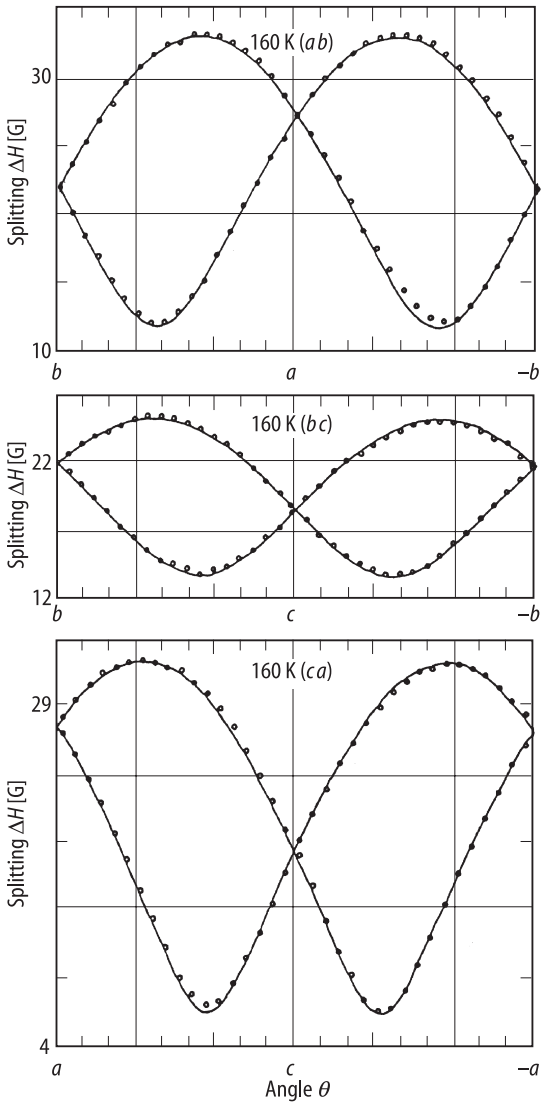

Fig. 41A-4-015. $CsLiSO_4$. ΔH vs. θ [87Hua]. T = 160 K. ΔH: hyperfine splitting of nitrogen. θ: angle between the magnetic field and crystallographic axes. Solid lines are numerical plot.

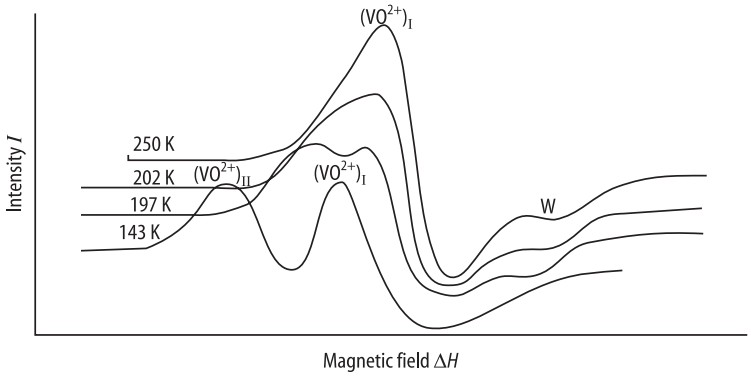

Fig. 41A-4-016. $CsLiSO_4$. I vs. ΔH [93Ana]. I: intensity of the hyperfine line of VO^{2+} along $H \parallel c$. ΔH: relative value of magnetic field. Parameter: T. W: a small but temperature dependent signal (197 K $\leq T \leq$ 250 K) indicating occurrence of a stable phase.

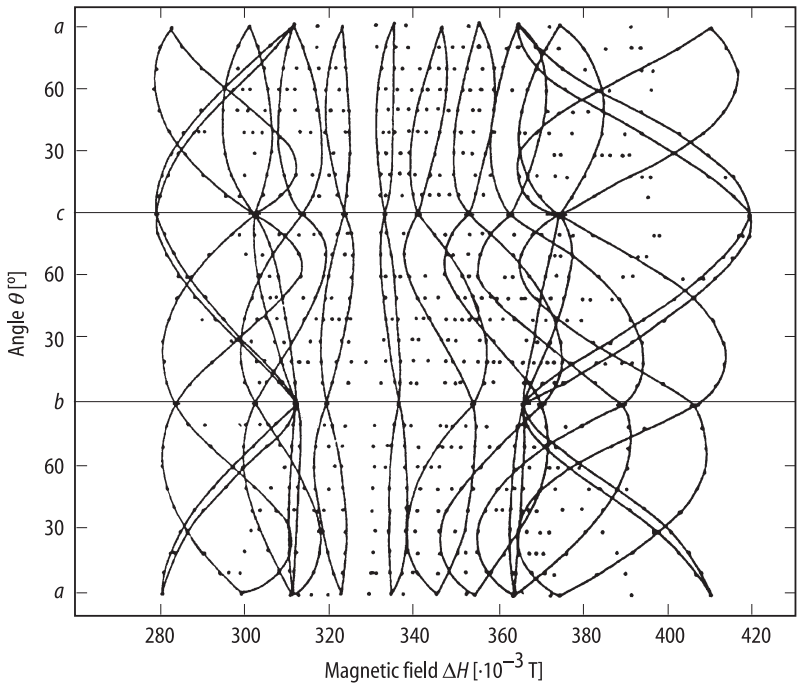

Fig. 41A-4-017. $CsLiSO_4$. θ vs. ΔH [93Ana]. T = RT. θ: angles [°] in the three orthogonal planes *ac*, *bc*, *ca*. ΔH: hyperfine resonance magnetic field.

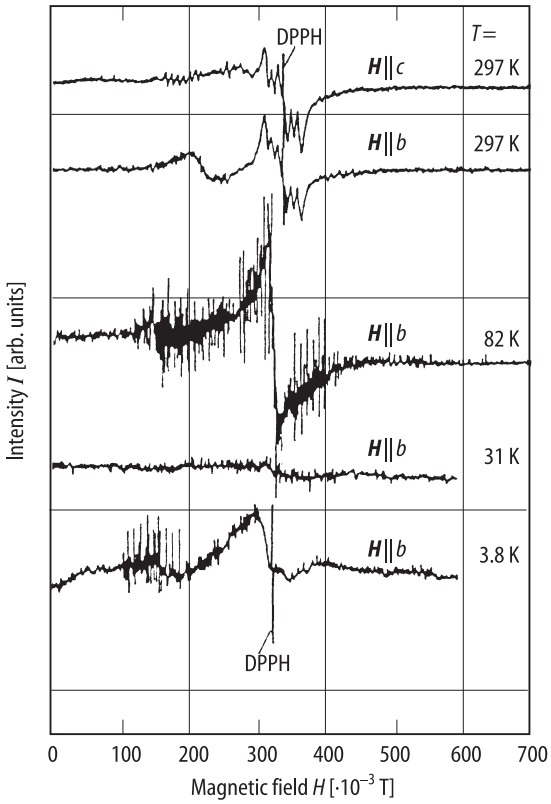

Fig. 41A-4-018. $CsLiSO_4$. I vs. H [93Mis]. I: electron paramagnetic resonance intensity of Mn^{2+} for $H \parallel c$ and $H \parallel b$. Parameter: T.

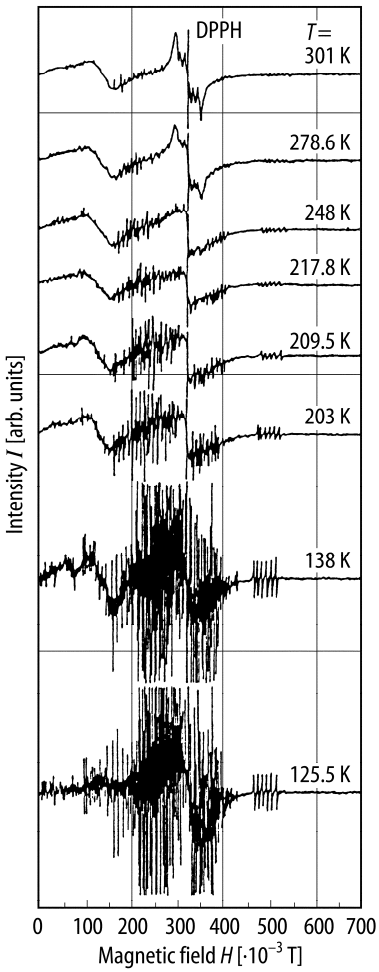

Fig. 41A-4-019. $CsLiSO_4$. I vs. H [93Mis]. I: electron paramagnetic resonance intensity of Mn^{2+} for H at –25° from the c axis in the ac plane. Parameter: T.

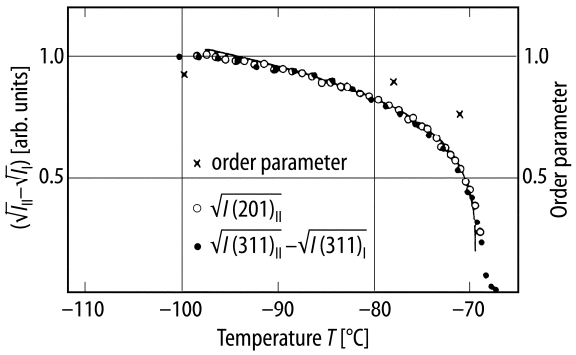

Fig. 41A-4-020. $CsLiSO_4$. ($\sqrt{I_{II}} - \sqrt{I_I}$) and order parameter vs. T [88Asa]. $I(201)_I = 0$.

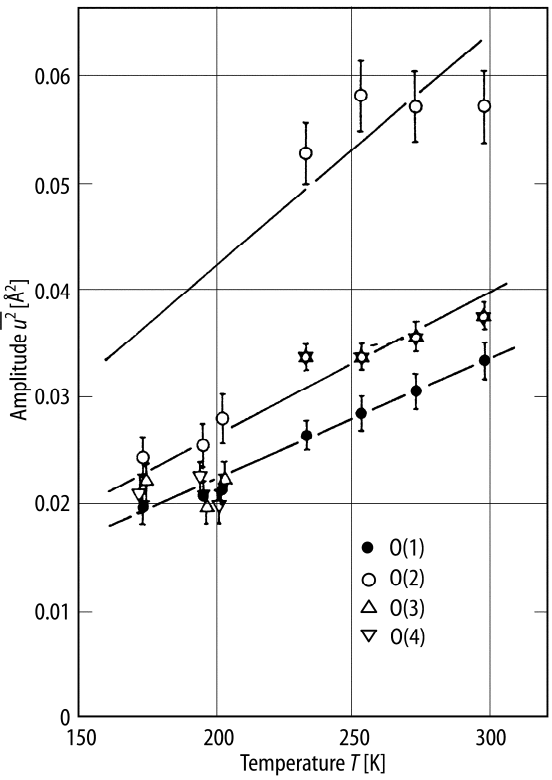

Fig. 41A-4-021. $CsLiSO_4$. $\overline{u^2}$ vs. T [88Asa]. $\overline{u^2}$: mean square amplitude of oxygens in the displacive-type model. The solid lines represent the relation $\overline{u^2} \propto T$. See also Table 41A-4-002.